Responses to Referee's Comments

Weakening of Antarctic Stratospheric Planetary in Early Austral Spring Since the Early 2000s: A Response to Sea Surface Temperature Trends

(ACP-2021-395)

Yihang Hu, Wenshou Tian, Jiankai Zhang, Tao Wang and Mian Xu

September 2021

Responses to Referee 1

The manuscript "Weakening of Antarctic Stratospheric Planetary Wave Activities in Early Austral Spring Since the Early 2000s: A Response to Sea Surface Temperature Trends" by Drs. Hu et al. identified a decreasing trend in the September Antarctic stratospheric wave activity since early 2000s and attribute it to the SST trends in the tropics and southern hemisphere. The modelling evidence presented in the manuscript well supports their conclusions and the paper is logically organized. It is thus recommended to be considered for publication after addressing the following comments:

Response:

We thank the reviewer for the helpful comments and valuable suggestions. We have revised the manuscript carefully according to the reviewer's comments and the detailed point-by-point responses to those comments are listed below.

Comment #1:

First of all, a positive trend in September Antarctic stratospheric wave activity is evident before 2000s (Fig. 2). It would be a more complete study to also simulate the 1980-2000 period similarly to better attribute and contrast the positive trend to the negative trend in the later period, as previous studies (e.g. Hu and Fu 2009) mostly use statistical methods for the attribution. This might require too much time and resource to complete and is thus only a suggestion.

Response:

Thanks for the comment. Hu and Fu (2009) (hereafter HF2009) simulated the trend of eddy heat flux under the observed time-varying SST (Fig. 11b in HF2009), which is relatively weak compared to that derived from reanalysis data (Fig. 6b in HF2009). However, they didn't show the trends of tropospheric wave sources in their paper. Fig. R1 shows the trends of stratospheric wave activities and tropospheric wave sources in September during 1980-2000 derived from MERRA-2 dataset. Note that the trends of stratospheric wave activities are not in accord with the trends of tropospheric wave

sources. The wave-1 component plays a predominate role in increase of stratospheric vertical wave flux during 1980-2000 (Fig. R1a, b). However, the trend of wave-1 component in 500 hPa geopotential height does not show a significant in-phase superposition on its climatology (Fig. R1e). The trend pattern of wave-2 component is in-phase with its climatology (Fig. R1f). These features in Fig. R1 imply that the wave-1 component of tropospheric wave sources was weakening during 1980-2000, while the wave-2 component was strengthening.

We have also conducted an model experiment (sstSHtrop80) forced by the linear increments of September SST during 1980-2000 over tropics and extratropical southern hemisphere (20°N-70°S), which is similar to sstSHtrop discussed in the manuscript. The applied SST anomalies are shown in Fig. R2. The responses of stratospheric wave activities and tropospheric wave sources to sstSHtrop80 are shown in Fig. R3. The responses of tropospheric wave sources are analogous to the trends derived from MERRA-2 to some extent. The response of wave-2 component is in-phase with its climatology (Fig. R3f), while the response of wave-1 component is out-of-phase with its climatology (Fig. R3e). The responses of stratospheric wave activities are consistent with the tropospheric wave sources. The response in wave-1 component is not significant (Fig. R3b), while the wave-2 component plays a dominate role in increase of stratospheric vertical wave flux in the model simulation (Fig. R3a, c). The results from sstSHtrop80 suggest that the SST increases over 20°N-70°S induce a strengthening of September stratospheric wave activity during 1980-2000. But it cannot explain the intensified wave-1 component of stratospheric wave activity shown in Fig. R1b.

Indeed, as the reviewer pointed out, a detailed attribution of the trend of Antarctic stratospheric wave activity during 1980-2000 needs much more efforts. In this manuscript, we mainly focuses on September wave activity after 2000, and some brief discussion about the the trend of Antarctic stratospheric wave activity before 2000 is added in the revised manuscript.

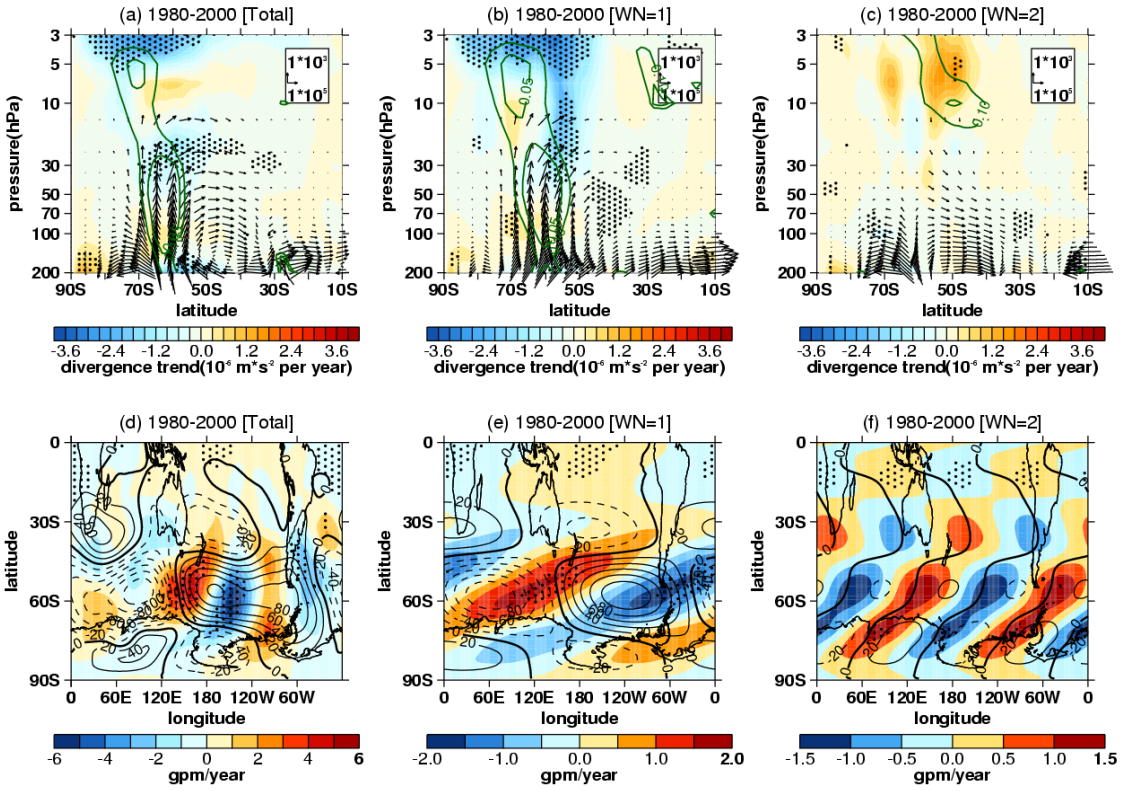

FIG. R1. (a-c) Trends of southern hemisphere (a) stratospheric E-P flux (arrows, units of horizontal and vertical components are 10^5 and 10^3 kg·s^{-2} per year, respectively) and its divergence (shadings) with their (b) wave-1 components and (c) wave-2 components over 1980-2000 in September derived from MERRA-2 dataset. (d-f) Trends (shadings) and climatological distributions (contours with an interval of 20 gpm, positive and negative values are depicted by solid and dashed lines respectively, zeroes are depicted by thick solid lines) of southern hemispheric (d) 500 hPa geopotential height zonal deviations with their (e) wave-1 component and (f) wave-2 component in September during 1980-2000 derived from MERRA-2 dataset. The stippled regions indicate the trends of E-P flux divergence or geopotential height significant at/above the 90% confidence level. The green contours from outside to inside (corresponding to p=0.1, 0.05) in Figs. R1a-c indicate the trend of vertical E-P flux significant at the 90% and 95% confidence level, respectively.

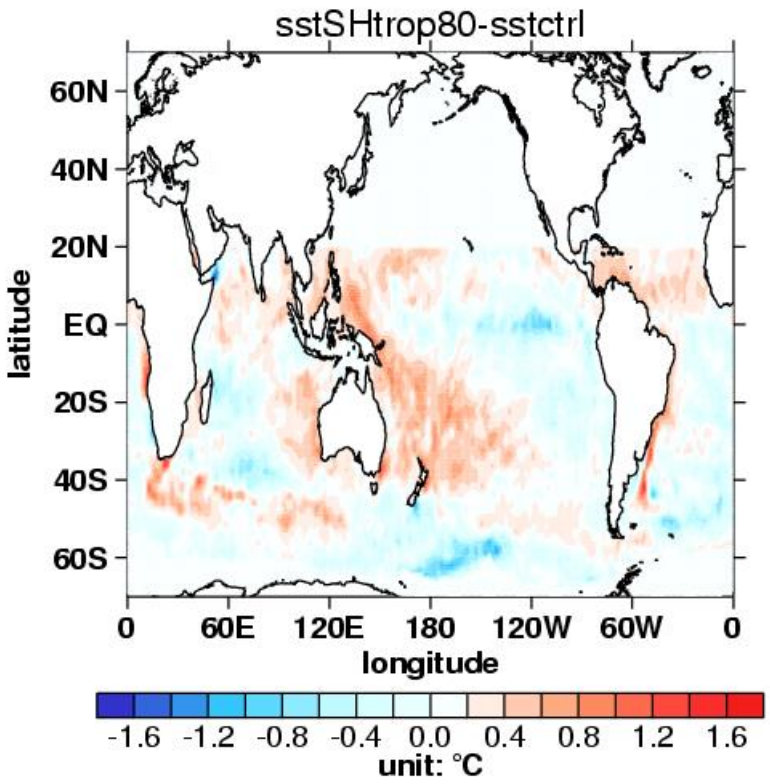

FIG. R2. Differences in SST forcing field between sstSHtrop80 and sstctrl.

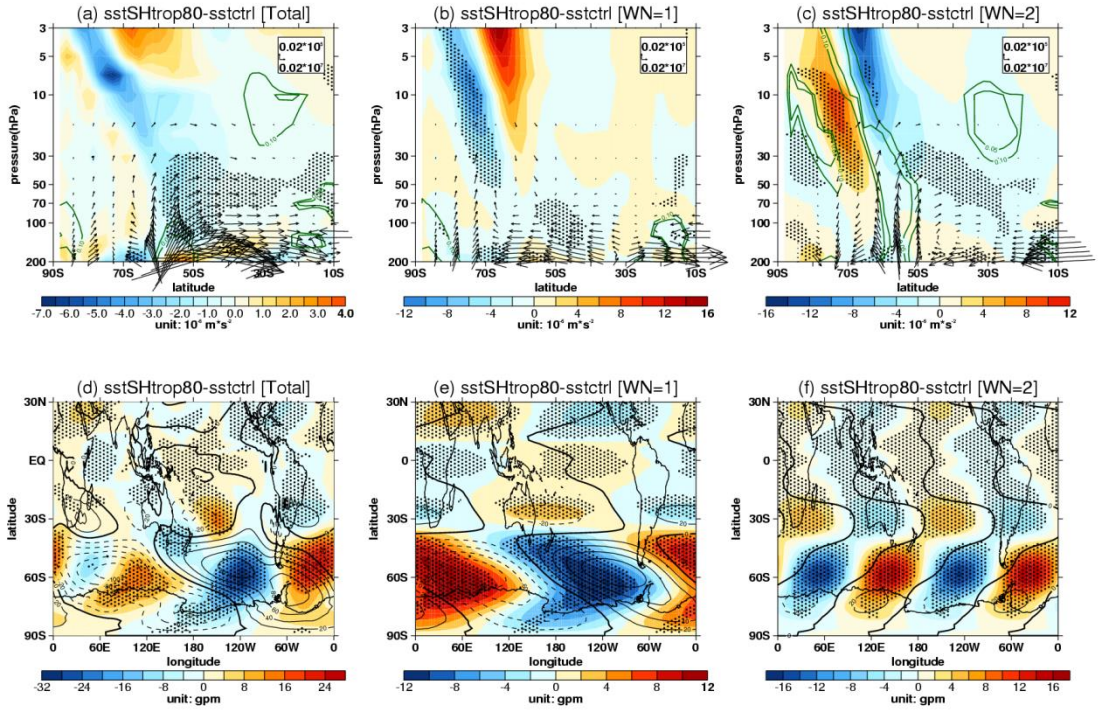

FIG. R3. Differences of (a) stratospheric E-P flux (arrows, units in horizontal and vertical components are 0.02×10^{7} and 0.02×10^{5} kg·s^{-2}, respectively) and its divergence (shadings) with their (b) wave-1 component and (c) wave-2 component between

sstSHtrop80 and sstctrl. Differences (shadings) of (d) 500 hPa geopotential height zonal deviations with their (e) wave-1 component and (f) wave-2 component between sstSHtrop80 and sstctrl. The mean distributions (contours with an interval of 20 gpm, positive and negative values are depicted by solid and dashed lines respectively, zeroes are depicted by thick solid lines) of geopotential height zonal deviations are derived from sstctrl. The stippled regions represent the mean differences significant at/above the 90% confidence level. The green contours from outside to inside in Figs. R3a-c represent the mean differences of vertical E-P flux significant at the 90% and 95% confidence levels.

Reference

Hu, Y., & Fu, Q.: Stratospheric warming in southern hemisphere high latitudes since 1979, Atmos. Chem. Phys., 9(13), 4329-4340, https://doi.org/10.5194/acp-9-4329-2009, 2009.

Comment #2:

Second, there is usually a time lag for the extratropical atmospheric circulation to respond to the tropical SST anomaly. The authors might need to justify whether it is reasonable to use September SST to drive the extratropical atmospheric circulation for the same month.

Response:

Thanks for the comment. We agree with the reviewer that there is a time lag for the extratropical atmosphere circulation to respond to tropical SST anomalies. As stated in the original manuscript (lines 244-245), the tropical SST anomalies (the linear increments) in experiment ssttrop are also applied in July and August (Fig. R4a, b) to avoid abrupt SST variations from month to month, and the two months are taken as spin-up time. Therefore, whether the SST forcing in July and August also contribute to the weakening of Antarctic stratospheric wave activity in September or not cannot be justified based on the experiment ssttrop only. Here, we performed an additional experiment ssttropAug without September SST anomalies (Fig. R4f) to clarify whether

the weakening of Antarctic stratospheric wave activity is induced by the tropical SST trend at the same month. Like other numerical experiments described in Table 1, the ssttropAug also includes 100 ensemble members that run from July to September forced by the same initial conditions from the 21st year to the 120th year in July generated by free run. The detailed descriptions of ssttropAug and other relevant experiments in the manuscript are displayed together in the Table R1 for comparison. The Figure R4 shows the applied global SST anomalies in ssttrop and ssttropAug from July to September.

The responses of tropospheric wave sources and stratospheric wave activities in ssttropAug are shown in Figs. R5a-c and Figs. R5d-f, respectively. Note that the anomalies of subpolar tropospheric geopotential height in September forced by changes in tropical SST in August does not superpose on their climatological patterns in an evident out-of-phase style (Figs. R5a-c). The anomaly of wave-1 component of geopotential height shows a slight in-phase overlap with its climatology over subpolar region (Fig. R5b). Accordingly, the responses of stratospheric wave activities over subpolar of southern hemisphere are not significant (Figs. R5d-f). The results here suggest that, the decrease of September vertical wave flux induced by SST changes in August is negligible comparing to that in the experiment with anomalous SST forcing in September (Figs. R5g), and the tropical SST trend in September plays a dominate role in weakening of stratospheric wave activity at the same month.

Furthermore, we also use a linear barotropic model (LBM) (e.g. Shaman & Tziperman, 2007; Shaman & Tziperman, 2011) to quantify the time scale for propagation of tropical anomalies to high latitudes. The LBM are developed to solve the barotropic vorticity equation, which is given as Eq. (1):

$$J(\bar{\psi}, \nabla^2\psi') + J(\psi', \nabla^2\bar{\psi} + f) + \alpha\nabla^2\psi' + K\nabla^4\nabla^2\psi' = R \tag{1}$$

where the Jacobian $J(A, B)$ is

$$J(A, B) = \frac{1}{r^2}\left(\frac{\partial A}{\partial \lambda}\frac{\partial B}{\partial \mu} - \frac{\partial A}{\partial \mu}\frac{\partial B}{\partial \lambda}\right) \tag{2}$$

the forcing function R is

$$R = -(f + \nabla^2\bar{\psi})D \tag{3}$$

ψ is the streamfunction, f is the Coriolis force, α is the Rayleigh coefficient, K is a diffusion coefficient, λ is longitude, $\mu = \sin(\theta)$, θ is latitude, r is the earth's radius and D is the divergence.

We use the wave-1 component of streamfunction derived from ensemble mean of sstctrl as the background field. In LBM, the initial anomaly is given by the divergence. We set $D = -7.9 \times 10^{-7}$ s^{-1}. The divergence forcing field is limited in 40°E-140°W, 10° S-0° (Fig. R6) to ensure the tropical initial anomaly of streamfunction superpose on its background field in an out-of-phase style. The LBM simulated streamfunction anomalies are shown in Figs. R7b-i. Note that the anomalies in tropics only take a few days to arrive the high latitudes in Southern Hemisphere. After about four days, a stable anti-phase superposition of streamfunction is well established in extratropical southern hemisphere (Figs. R7f-i). These results are supported by previous studies (e.g. Shaman & Tziperman, 2011), which also indicate that the horizontal propagation of anomaly in atmosphere takes a few days.

Previous studies also reported that it takes about 4 days for wave-1 to propagate from troposphere into stratosphere and 1-2 days for wave-2 (e.g. Randel, 1987). We agree with the reviewer that the tropical oceans affect the stratosphere at mid-high latitudes with a lag of several days. However, the SST forcing field applied in CESM is on monthly scale. It is reasonable to use September SST trend to drive and explain the trends of extratropical circulation and wave activity at the same month.

Table R1. Configurations of sstctrl, ssttrop and ssttropAug.

Experiments	Descriptions
sstctrl	Control run. Seasonal cycle of monthly mean global SST data over 1980-2000 is derived from the ERSST v5 dataset. Fixed values of ozone, greenhouse gases and aerosol fields in 2000 are used.
ssttrop	As in sstctrl, but with linear increments of SST in September over 2000-2017 superposed on the tropics (20°S-20°N). As shown in

	Fig. R1a-c, the global SST anomalies are applied from July to September,.
ssttropAug	As in sstctrl, but with linear increments of SST in August over 2000-2017 superposed on the tropics (20°S-20°N). As shown in Fig R1d-f, the SST anomalies are only applied from July to August.

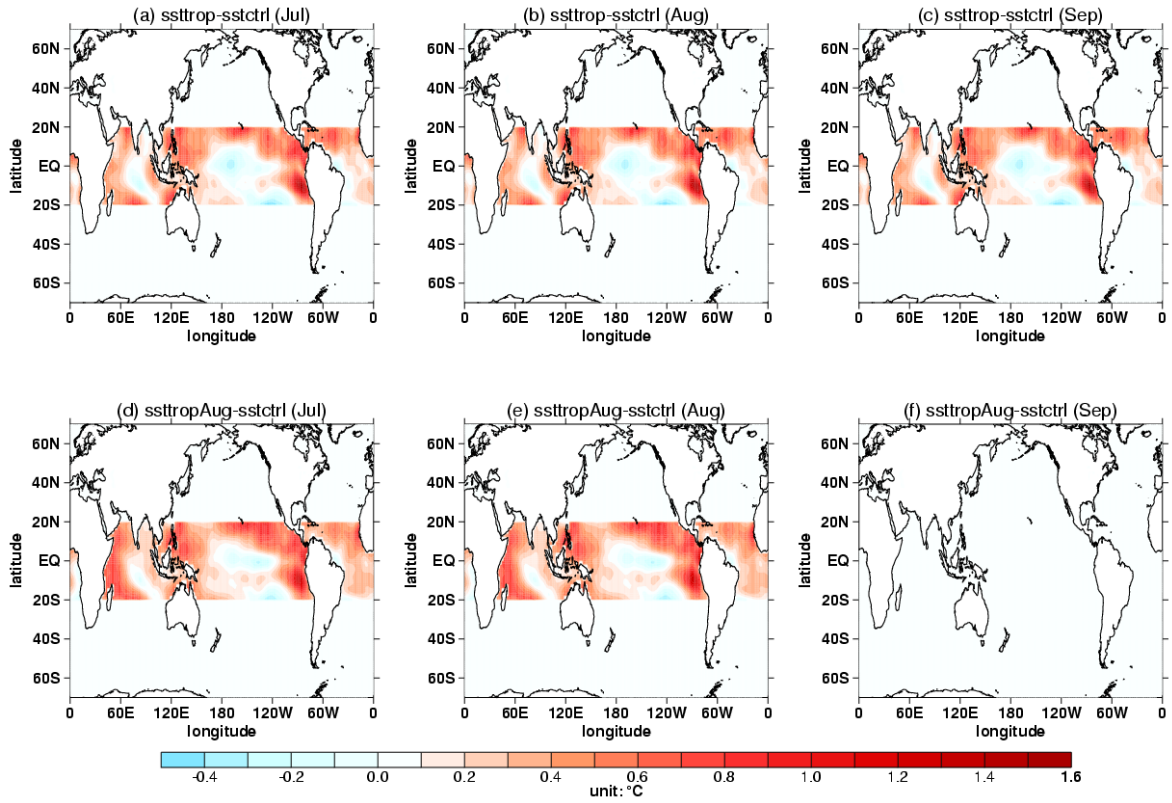

FIG. R4. Differences of SST forcing fields in July (a, d), August (b, e) and September (c, f) between the sensitive experiments ((a, b, c) ssttrop; (d, e, f) ssttropAug) and the control experiment (sstctrl).

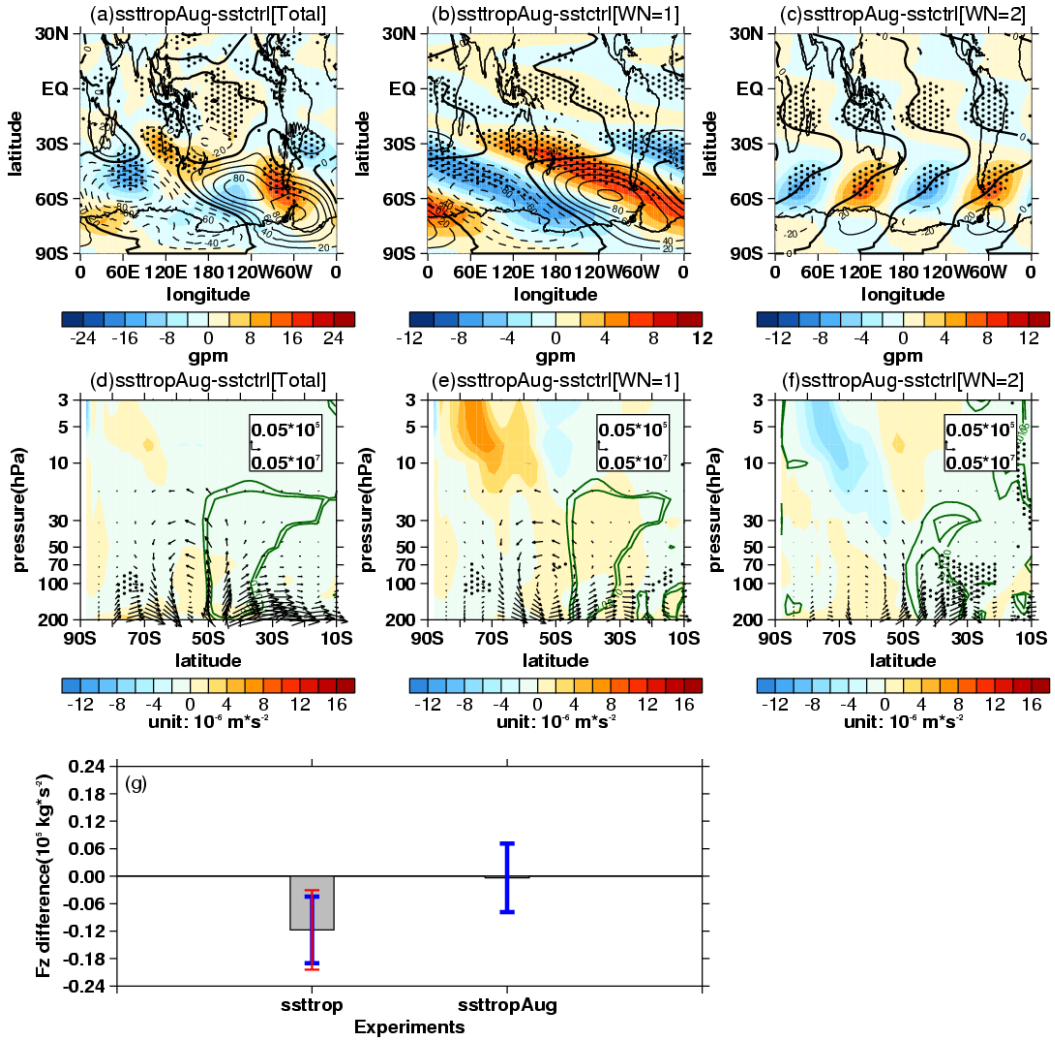

FIG. R5. (a-c) The responses of tropospheric wave sources in experiment ssttropAug: differences of (a) 500 hPa geopotential height zonal deviations with their (b) wave-1 component and (c) wave-2 component between ssttropAug and sstctrl. The mean distributions (contours with an interval of 20 gpm, positive and negative values are depicted by solid and dashed lines, respectively, zeros are depicted by thick solid lines) of them are derived from sstctrl. (d-f) The responses of stratospheric wave activities in experiment ssttropAug: differences of (d) stratospheric E-P flux (arrows, units in horizontal and vertical components are 0.05×10^7 and 0.05×10^5 kg·s^{-2}, respectively) and its divergence (shadings) with their (e) wave-1 component and (f) wave-2 component between ssttropAug and sstctrl. The stippled regions in Figs. R5a-f represent the mean difference significant at/above the 90% confidence level. The green contours from outside to inside (corresponding to p=0.1 and 0.05) in Figs. R5d-f represent the mean

differences of vertical E-P flux significant at the 90% and 95% confidence levels, respectively. (g) Mean differences (grey pillars) and corresponding uncertainties (error bars) of Fz (area-weighted from 200 hPa to 10 hPa over 70°S-50°S) between sensitive experiments and the control experiment. The blue and red error bars reflect the 90% and 95% confidence levels calculated by two-tailed t test, respectively.

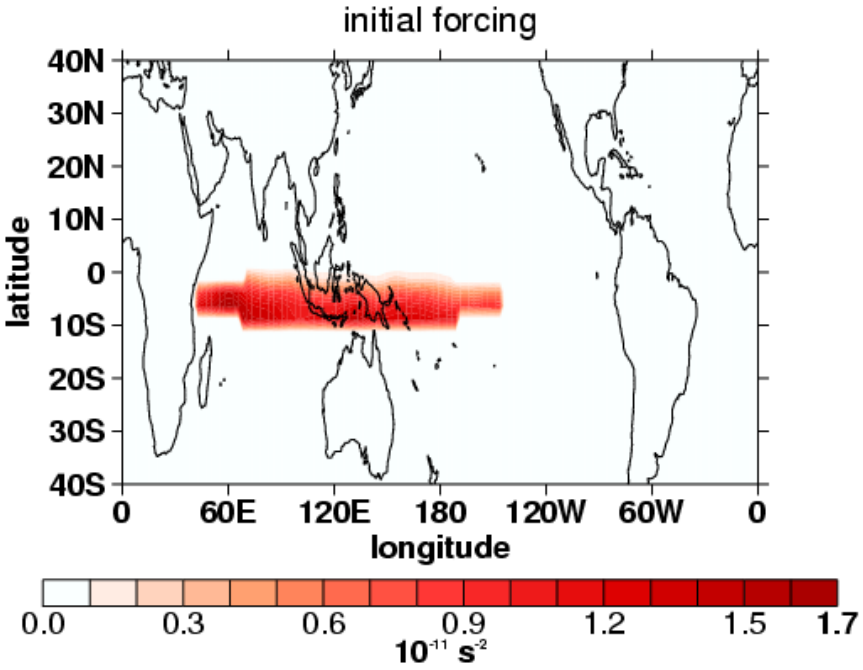

FIG. R6. The initial forcing ($R = -(f + \nabla^2\bar{\psi})D$) distribution in LBM.

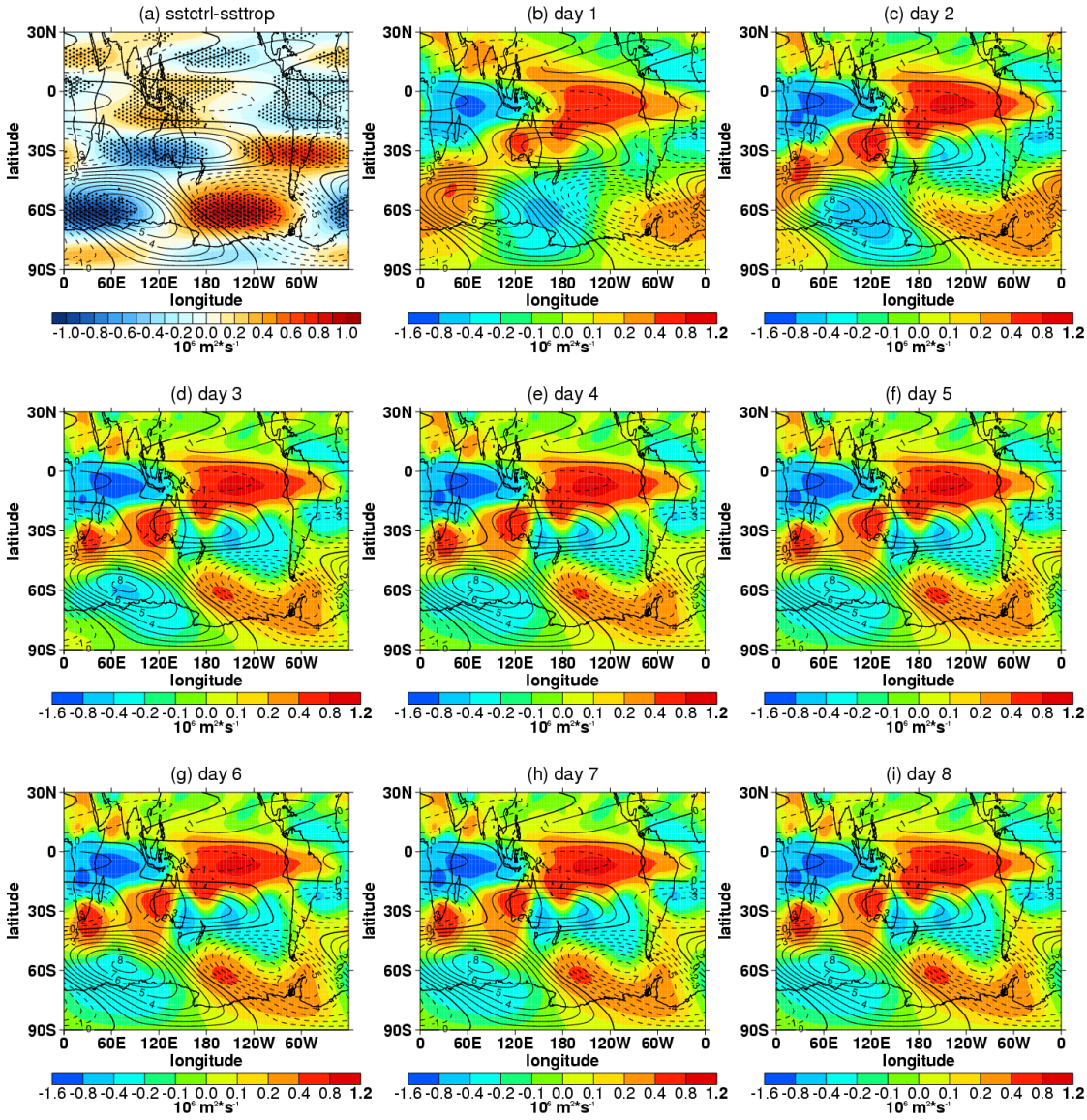

FIG. R7. The background field (contours with interval of 10^6 $m^2 \cdot s^{-1}$, positive and negative values are depicted by solid and dashed lines, respectively, zeros are depicted by thick solid lines) of streamfunctions derived from sstctrl and the responses (shading) of streamfunctions derived from (a) ssttrop in CESM and (b-i) the first to eighth model days in LBM.

Reference

Randel, W. J.: A study of planetary waves in the southern winter troposphere and stratosphere. Part I: Wave structure and vertical propagation, J. Atmos. Sci., 44(6), 917-935, 1987.

Shaman, J., & Tziperman, E.: Summertime ENSO-North African-Asian Jet teleconnection and implications for the Indian monsoons, Geophys. Res. Lett., 34(11), L11702, https://doi.org/

10.1029/2006GL029143, 2007.

Shaman, J., & Tziperman, E.: An atmospheric teleconnection linking ENSO and southwestern European precipitation, J. Climate., 24(1), 124-139, https://doi.org/10.1175/2010JCLI3590.1, 2011.

Comment #3:

Last, it would be nice to show the simulated EP-flux time series as in Fig. 2 but forced by SSTs to visualize how significant that is compared with the EP-flux trends in reanalysis datasets. Previous studies (e.g. Wang and Waugh, 2012, https://doi.org/10.1029/2011JD017130) found that the extratropical stratospheric wave activity trend is difficult to capture using model simulations with small ensembles. It might help to illustrate the benefit of using large ensembles as in this study.

Response:

Thanks for the comment. The study (hereafter WW2012) mentioned in this comment uses the chemistry-climate model simulations to evaluate the trends of stratospheric temperature, residual circulation as well as wave activity during recent decades (Wang and Waugh, 2012). These simulations are all forced by time varying SSTs, GHGs and ODSs. It's necessary to emphasize that the simulations conducted in our study are all time-slice experiments. We had tried to conduct transient experiments forced by time-varying SST derived from ERSST v5. However, possibly due to the limitation of the model performance, the trends of wave activities we simulated are not significant despite the opposite signs during 1980-2000 and 2000-2018 (Table R2, Fig. R8), which is analogous to Fig. 6 in WW2012. Meanwhile, numerous previous studies also used time-slice experiments to attribute the trends in atmosphere (e.g. Hu et al., 2018; Kang et al., 2011; Zhang et al., 2016) and we perform time-slice experiments mainly for the purpose of attribution rather than generating a real trend. Fig. R9 shows the simulated stratospheric vertical wave flux derived from each ensemble member in our study. Although the scatter plots do not show clear trends like Fig. 2 in manuscript, the differences between ensemble means in values of these dots still indicate the

decrease of stratospheric wave activities induced by SST changes.

Table R2. Trends of stratospheric vertical wave flux time series (averaged from 100 hPa to 30 hPa over 70°S-50°S) derived from different transient experiments (tr01, tr02, tr03, tr04, tr05) and ensemble mean of them on piecewise periods (1980-2000 and 2000-2018).

	tr01	tr02	tr03	tr04	tr05	ensemble mean
1980-2000	0.0091 (p=0.44)	-0.012 (p=0.32)	0.012 (p=0.15)	0.0031 (p=0.67)	0.0034 (p=0.77)	0.0031 (p=0.55)
2000-2018	-0.0060 (p=0.61)	0.0086 (p=0.67)	-0.030 (p=0.039)	-0.0034 (p=0.87)	0.019 (p=0.23)	-0.0023 (p=0.76)

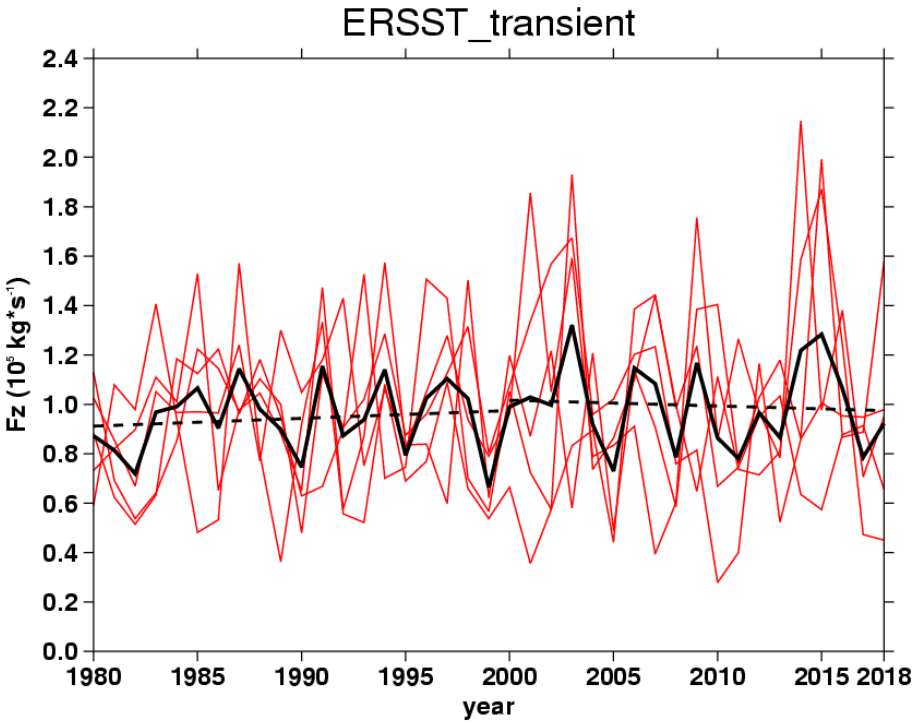

FIG. R8. Time series (solid lines) of vertical E-P flux area-weighted from 100 hPa to 30 hPa over 70°S-50°S in September during 1980-2018 derived from simulations forced by time-varying SST. Five different red solid lines stand for the time series driven by different initial conditions and the black solid line represent the ensemble

mean of them. The straight dashed lines show linear regressions to the ensemble mean on two piecewise period (1980-2000 and 2000-2018).

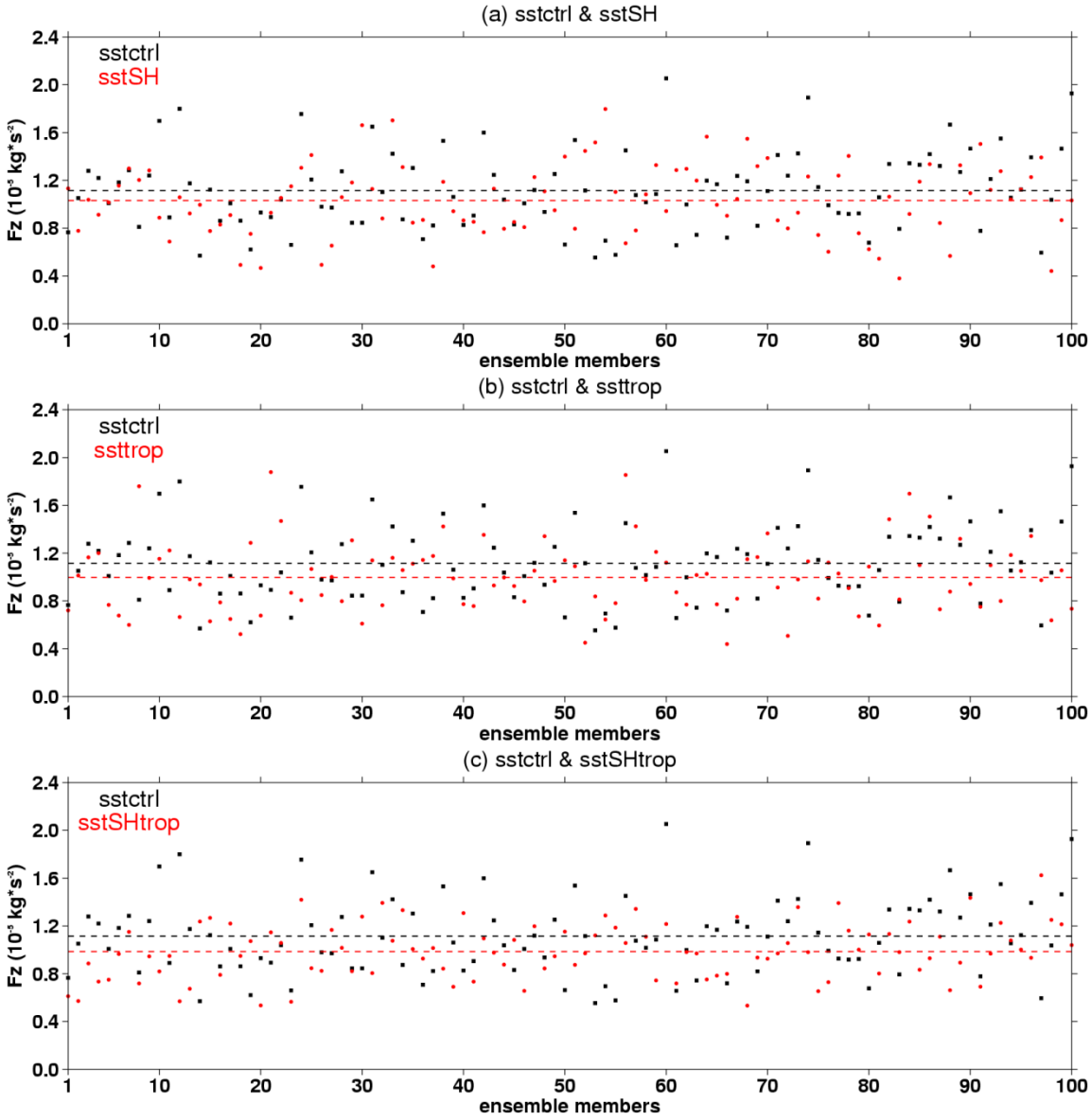

FIG. R9. Stratospheric vertical E-P flux (Fz, area-weighted from 200 hPa to 10 hPa over 70°S-50°S) derived from each ensemble member of control experiment (black squares) and different sensitive experiment (red circles; (a) sstSH; (b) ssttrop; (c) sstSHtrop). Black and red horizontal dashed lines represent the ensemble means derived from control experiment and sensitive experiments, respectively.

Reference

Hu, D., Guan, Z., Tian, W., & Ren, R.: Recent strengthening of the stratospheric Arctic vortex

response to warming in the central North Pacific, Nat. Commun., 9(1), 1697. https://doi.org/10.1038/s41467-018-04138-3, 2018.

Kang, S. M. , Polvani, L. M. , Fyfe, J. C. , & Sigmond, M.: Impact of polar ozone depletion on subtropical precipitation, Science, 332(6032), 951-954, https://doi.org/10.1126/science.1202131, 2011.

Wang, L., & Waugh, D., W.: Chemistry-climate model simulations of recent trends in lower stratospheric temperature and stratospheric residual circulation, J. Geophys. Res-Atmos., 117(D9), https://doi.org/10.1029/2011JD017130, 2012.

Zhang, J., Tian, W. , Chipperfield, M. P. , Xie, F. , & Huang, J.: Persistent shift of the arctic polar vortex towards the eurasian continent in recent decades, Nat. Clim. Change. 6, 1094–1099. https://doi.org/10.1038/nclimate3136, 2016.